2023 IEEE International Conference on Robotics and Automation (ICRA 2023)
May 29 - June 2, 2023. London, UK

Finding the Optimal Incision Point in Robotic Assisted Surgery

Kyriakos Almpanidis, Theodora Kastritsi and Zoe Doulgeri

Abstract— **In robotic assisted surgeries, surgical tools are inserted into the human body via an incision point in the abdominal wall, which is imposed as a remote center of motion (RCM). The selection of the incision's point location in the human body is critical for the success of the surgical procedure. In this paper, we propose a simulation tool for finding the optimal incision point location, which can be utilized by the surgeon during the preoperative stage. The surgeon can plan the path/region of intervention as well as sensitive regions which should be protected from unintentional damage by the surgical tool on the preoperative images of internal organs. A target admittance model that enforces a candidate incision as a RCM is utilized in the simulation enhanced by a term for following the planned path. We propose a cost evaluation function taking into account metrics involving the distance of the tool from sensitive areas, the tool links maximum pressure on tumors and the robot's dexterity measure. The example of a tumor resection task is used with the simulation tool to demonstrate its use in finding the incision points that ensures minimal intraoperative risks and accurate task execution.**

Index Terms— **Robot assisted minimal invasive surgery, Simulation tool, Remote Center of Motion, Evaluation function**

I. INTRODUCTION

In robot assisted minimally invasive surgeries, surgical tools are inserted inside the patient's body through small incisions in the abdominal wall. Thus, it is important for an incision point to be imposed as a remote center of motion (RCM) to ensure minimum stress and injury to the incision wall. This constraint reduces by two the robot's dof and thus the tool shaft motion is only free to translate and rotate along and around its axis as well as rotate around the RCM. Surgical instruments do usually provide extra dofs at the end of the shaft in order to enable the surgeon to place the instrument tip to a desired pose.

In some specially developed surgical robots, the RCM constraint is achieved through mechanisms which ensure that the tool passes through the incision point during the surgical task. In the case of utilizing a general purpose manipulator, the RCM should be imposed by control-based strategies [1]. Different methods have been proposed for actively imposing the RCM constraint. In our previous work [2], [3] a target admittance model that enforces RCM on the tool shaft and decouples the constrained and free space is proposed for hands-on manipulation. In both cases, the location of the insertion point is critical for accurate task execution.

Few papers focus on the problem of selecting an the optimal incision point location. In [4] a redundant manipulator is considered with a surgical tool attached to its tip and the RCM evaluation is based on an isotropy index. This work does not take into account other metrics such as the distance from sensitive areas which is critical in surgical procedures. In [5], a framework is proposed for selecting the position of the optimal incision point utilizing Hierarchical Quadrattic Programming. In the evaluation of the candidate incision, the path following errors, the distance from nearby organs, the robot's dexterity and the tool's insertion angle wrt the torso are used. However, the proposed cost function contains products and quotients of the evaluation metrics; thus much greater importance is given to the metric that has the dominant value.

Thus far, the metrics for selecting the optimal incision point focuses mainly on the system's performance, sensitive organs proximity and task's accuracy. None of the previous works consider inadvertent cuts of tumors in their evaluation metrics, which are however known to be correlated with cancer's recurrence and metastasis [6].

The main aim of this work is to provide a simulation tool for finding the optimal incision point location which minimizes both intra-operative and postoperative risks and is demonstrated in a tumor resection task. A region for candidate incision points, a predesigned oriented path and forbidden regions of sensitive organs are given as inputs to the simulation model. A general purpose manipulator on which an articulated tool is attached to its wrist is considered. The simulated robot's motion is based on the target admittance model of [3] which is enhanced by a term that ensures tracking of the desired oriented path. We propose a cost function which is taking into account metrics related to the distance from sensitive areas, the tool's pressure on the tumor, the robot's isotropy and the accuracy of following the pre-planned path. Candidate incision points from a predefined region are evaluated with the proposed cost function to find the optimal.

II. ROBOTIC CHAIN KINEMATICS

Consider a general purpose manipulator with n-dof. Let $\boldsymbol{q}_k, \dot{\boldsymbol{q}}_k \in \mathbb{R}^n$ denote its joint positions and velocities respectively. We place the inertial frame $\{0\}$ at its base and let $\{\mathrm{w}\}$ be the frame of its wrist with rotation matrix $\boldsymbol{R}_w = \begin{bmatrix}\boldsymbol{x}_w & \boldsymbol{y}_w & \boldsymbol{z}_w\end{bmatrix}$. Let an articulated tool with a long tool shaft followed by m-joints, like the one described in [7], be rigidly attached to its wrist with the tool shaft placed along axis $\boldsymbol{x}_w$ without loss of generality as shown in Fig. 1. Let $\boldsymbol{q}_\alpha, \dot{\boldsymbol{q}}_\alpha \in \mathbb{R}^m$ denote its joint positions and velocities respectively. Let frame $\{\mathrm{s}\}$ be attached at the end of the tool shaft of the articulated tool with $\boldsymbol{p}_s$, $\boldsymbol{R}_s = \begin{bmatrix}\boldsymbol{x}_s & \boldsymbol{y}_s & \boldsymbol{z}_s\end{bmatrix}$

The authors are with the Department of Electrical and Computer Engineering, Aristotle University of Thessaloniki, Thessaloniki, 54124, Greece: aakyriako@ece.auth.gr, tkastrit@gmail.com, doulgeri@ece.auth.gr

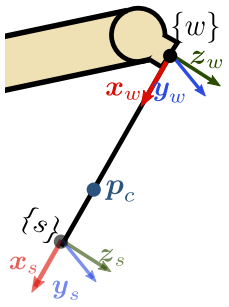

Fig. 1. Robot with the tool shaft

denoting its position and orientation and $\boldsymbol{J}_s \in \mathbb{R}^{6\times n}$ the respective robot Jacobian. Let frame {e} be attached at the tip of the articulated tool with $\boldsymbol{p}_e$, $\boldsymbol{R}_e$ denoting its position and orientation and $\boldsymbol{p}_{se}$, $\boldsymbol{R}_{se}$ the tip's position and orientation with respect to the frame $\{s\}$. Frame $\{s\}$ can be considered the basis frame of the tool's articulated part. Let $\boldsymbol{J}_{se} \in \mathbb{R}^{6\times m}$ denote the Jacobian matrix of the articulated part mapping the joint velocities of the articulated instrument to the tool tip generalized velocity wrt to frame $\{s\}$. Thus the robot and the tool form a robotic chain with a total of $n+m$ dof. Then the following kinematic relationships hold:

$$\boldsymbol{p}_e = \boldsymbol{p}_s + \boldsymbol{R}_s \boldsymbol{p}_{se} \tag{1}$$

$$\boldsymbol{R}_e = \boldsymbol{R}_s \boldsymbol{R}_{se} \tag{2}$$

Differentiating (1), utilizing $\hat{\boldsymbol{\omega}}_s = \dot{\boldsymbol{R}}_s \boldsymbol{R}_s^T \Leftrightarrow \dot{\boldsymbol{R}}_s = \hat{\boldsymbol{\omega}}_s \boldsymbol{R}_s$, where $(.)^\wedge$ is the skew-symmetric operator and $\boldsymbol{\omega}_s$ the rotational velocity of the tool shaft yields:

$$\dot{\boldsymbol{p}}_e = \dot{\boldsymbol{p}}_s + \boldsymbol{R}_s \dot{\boldsymbol{p}}_{se} - (\boldsymbol{R}_s \boldsymbol{p}_{se})^\wedge \boldsymbol{\omega}_s \tag{3}$$

Differentiating (2), utilising the properties $\dot{\boldsymbol{R}}_{se} = \hat{\boldsymbol{\omega}}_{se} \boldsymbol{R}_{se}$ and $\dot{\boldsymbol{R}}_s = \hat{\boldsymbol{\omega}}_s \boldsymbol{R}_s$ yields:

$$\dot{\boldsymbol{R}}_e = \hat{\boldsymbol{\omega}}_s \boldsymbol{R}_e + \boldsymbol{R}_s \hat{\boldsymbol{\omega}}_{se} \boldsymbol{R}_{se} \tag{4}$$

Then, the rotational velocity of the tip of the articulated tool $\boldsymbol{\omega}_e$ utilizing the property $\hat{\boldsymbol{\omega}}_e = \dot{\boldsymbol{R}}_e \boldsymbol{R}_e^T$ is given by $\hat{\boldsymbol{\omega}}_e = \hat{\boldsymbol{\omega}}_s + \boldsymbol{R}_s \hat{\boldsymbol{\omega}}_{se} \boldsymbol{R}_s^T$ which can be rewritten as:

$$\boldsymbol{\omega}_e = \boldsymbol{\omega}_s + \boldsymbol{R}_s \boldsymbol{\omega}_{se} \tag{5}$$

Splitting the Jacobians $\boldsymbol{J}_s$ and $\boldsymbol{J}_{se}$ into their translational and rotational parts $\boldsymbol{J}_{s_v}, \boldsymbol{J}_{s_\omega} \in \mathbb{R}^{3\times n}$ and $\boldsymbol{J}_{se_v}, \boldsymbol{J}_{se_\omega} \in \mathbb{R}^{3\times m}$ respectively, the following mappings from the related joint spaces hold; $\dot{\boldsymbol{p}}_s = \boldsymbol{J}_{s_v} \dot{\boldsymbol{q}}_k, \boldsymbol{\omega}_s = \boldsymbol{J}_{s_\omega} \dot{\boldsymbol{q}}_k$ and $\dot{\boldsymbol{p}}_{se} = \boldsymbol{J}_{se_v} \dot{\boldsymbol{q}}_\alpha$, $\boldsymbol{\omega}_{se} = \boldsymbol{J}_{se_\omega} \dot{\boldsymbol{q}}_\alpha$. Utilising the above relationships in (3) and (5), we can find the Jacobian of the combined robotic chain, mapping the joint velocities to the generalized velocity of the tip $\boldsymbol{V}_e \in \mathbb{R}^6$:

$$\boldsymbol{V}_e = \begin{bmatrix} \dot{\boldsymbol{p}}_e \\ \boldsymbol{\omega}_e \end{bmatrix} = \boldsymbol{J}_e \begin{bmatrix} \dot{\boldsymbol{q}}_k \\ \dot{\boldsymbol{q}}_\alpha \end{bmatrix} \tag{6}$$

$$\boldsymbol{J}_e = \begin{bmatrix} \boldsymbol{J}_{s_v} - (\boldsymbol{R}_s \boldsymbol{p}_{se})^\wedge \boldsymbol{J}_{s_\omega} & \boldsymbol{R}_s \boldsymbol{J}_{se_v} \\ \boldsymbol{J}_{s_\omega} & \boldsymbol{R}_s \boldsymbol{J}_{se_\omega} \end{bmatrix} \in \mathbb{R}^{6\times(n+m)}$$

The left pseudo-inverse of Jacobian $\boldsymbol{J}_e$ which satisfies $\boldsymbol{J}_e \boldsymbol{J}_e^\dagger = \boldsymbol{I}_{6\times 6}$ can be found by the following expression when the robot is moving away from any singularities $\boldsymbol{J}_e^\dagger = \boldsymbol{J}_e^T (\boldsymbol{J}_e \boldsymbol{J}_e^T)^{-1} \in \mathbb{R}^{(n+m)\times 6}$.

III. Target admittance model enforcing RCM: Preliminaries

In our previous work [3], a static RCM is enforced in a general purpose manipulator holding a long tool shaft via the appropriate design of a target admittance model which in addition decouples the constrained and unconstrained space. We briefly present the model in this section. Let the incision point be denoted by $\boldsymbol{p}_c$. Then the projection of the vector $\boldsymbol{p}_s - \boldsymbol{p}_c$ on the plane with basis $\boldsymbol{B} = \begin{bmatrix} \boldsymbol{y}_w & \boldsymbol{z}_w \end{bmatrix} \in \mathbb{R}^{3\times 2}$, which is vertical to $\boldsymbol{x}_w$, yields the constraint coordinates $\boldsymbol{x}_c = \boldsymbol{B}^T (\boldsymbol{p}_s - \boldsymbol{p}_c) \in \mathbb{R}^{2\times 1}$ and the respective constraint velocity $\dot{\boldsymbol{x}}_c = \boldsymbol{A}_c \begin{bmatrix} \dot{\boldsymbol{p}}_s^T & \boldsymbol{\omega}_s^T \end{bmatrix}^T$ where $\boldsymbol{A}_c = \boldsymbol{B}^T \begin{bmatrix} \boldsymbol{I}_{3\times 3} & (\boldsymbol{p}_s - \boldsymbol{p}_c)^\wedge \end{bmatrix} \in \mathbb{R}^{2\times 6}$ is the constraint Jacobian in the task space. Both $\boldsymbol{x}_c$ and $\dot{\boldsymbol{x}}_c$ should be ideally zero for constraint enforcement. The constraint velocity in the joint space is then given by:

$$\dot{\boldsymbol{x}}_c = \boldsymbol{A} \dot{\boldsymbol{q}}_k \in \mathbb{R}^2 \tag{7}$$

with $\boldsymbol{A} = \boldsymbol{A}_c \boldsymbol{J}_s \in \mathbb{R}^{2\times n}$ is the joint space constraint Jacobian. Let $\boldsymbol{Z} \in \mathbb{R}^{(n-2)\times n}$ denote the basis of the unconstrained space so that $\boldsymbol{A}\boldsymbol{Z}^T = \boldsymbol{0}_{2\times(n-2)}$. We can then write the target admittance model proposed in [3] in a combined form and with zero free space damping as follows:

$$\ddot{\boldsymbol{q}}_k = -\boldsymbol{S} \begin{bmatrix} \boldsymbol{h}_1 \\ \boldsymbol{h}_2 - \boldsymbol{u}_c \end{bmatrix} \tag{8}$$

where $\boldsymbol{h}_1 = \dot{\boldsymbol{A}} \dot{\boldsymbol{q}}_k + 2a \dot{\boldsymbol{x}}_c + a^2 \boldsymbol{x}_c \in \mathbb{R}^2, \boldsymbol{h}_2 = \frac{d(\boldsymbol{Z}^{\dagger T})}{dt} \dot{\boldsymbol{q}}_k \in \mathbb{R}^{n-2}, \boldsymbol{S} = [\boldsymbol{A}^\dagger \ \boldsymbol{Z}^T] \in \mathbb{R}^{n\times n}$ with a being a positive gain, $\boldsymbol{A}^\dagger \in \mathbb{R}^{n\times 2}$ the left pseudoinverse of $\boldsymbol{A}$ i.e. $\boldsymbol{A}\boldsymbol{A}^\dagger = \boldsymbol{I}_{2\times 2}$, and $\boldsymbol{u}_c \in \mathbb{R}^{(n-2)}$ being an input term that determines the unconstrained space dynamics. Notice that the inverse of the square matrix $\boldsymbol{S}$ is given analytically by:

$$\boldsymbol{S}^{-1} = [\boldsymbol{A}^T \ \boldsymbol{Z}^\dagger]^T \in \mathbb{R}^{n\times n}$$

where $\boldsymbol{Z}^{\dagger T} \in \mathbb{R}^{(n-2)\times n}$ is the right pseudoinverse of $\boldsymbol{Z}^T$ i.e $\boldsymbol{Z}^{\dagger T} \boldsymbol{Z}^T = \boldsymbol{I}_{(n-2)\times(n-2)}$. Left multiplying (8) by $\boldsymbol{S}^{-1}$ we can recover the decoupled dynamics of the constrained and unconstrained space. The constrained motion dynamics are given by the linear homogeneous differential equation:

$$\ddot{\boldsymbol{x}}_c + 2a \dot{\boldsymbol{x}}_c + a^2 \boldsymbol{x}_c = \boldsymbol{0}_{2\times 1} \tag{9}$$

which ensures exponential convergence to zero with a speed determined by the value of gain a in the presence of initial non-zero values; for zero initial conditions which we assume in this work, the solution is identical to zero for all times i.e. the model guarantees the RCM constraint satisfaction.

The unconstrained space dynamics on the other hand are given by:

$$\ddot{\boldsymbol{x}}_f = \boldsymbol{u}_c \tag{10}$$

where $\dot{\boldsymbol{x}}_f = \boldsymbol{Z}^{\dagger T} \dot{\boldsymbol{q}}_k \in \mathbb{R}^{n-2}$ is the velocity of the unconstrained space.

Hence the unconstrained space dynamics are determined by $\boldsymbol{u}_c \in \mathbb{R}^{(n+m-2)}$ which can be the human force in hands-on manipulation or any term that can be designed to achieve a feasible tracking objective as in [8].

IV. Extension of target admittance model for oriented path tracking

Let the instrument's tip position trajectory be denoted by $\boldsymbol{p}_d(t) \in \mathbb{R}^3$ and the orientation by $\boldsymbol{Q}_d(t) \in \mathbb{S}^3$ in the unit quaternion form. These trajectories define an oriented path which is designed by the surgeon on the preoperative environment. Initially we assume that the tool shaft passes through the incision point. It is also assumed that initially the tool shaft does not touch any forbidden regions. Define the position tracking error as $\widetilde{\boldsymbol{p}}_e = \boldsymbol{p}_e - \boldsymbol{p}_d \in \mathbb{R}^3$ and the orientation error as $\boldsymbol{e}_q = 2\widetilde{n}\widetilde{\boldsymbol{e}} \in \mathbb{R}^3$ with $\widetilde{n}, \widetilde{\boldsymbol{e}}$ being the scalar and the vector part of the orientation error quaternion $\widetilde{\boldsymbol{Q}} = \boldsymbol{Q}_e * \boldsymbol{Q}_d$ where $*$ denotes the quaternion product. This is one of the expressions for the orientation error that is utilized in the literature [9]. Notice the $\widetilde{\boldsymbol{Q}}$ corresponds to the rotation matrix $\widetilde{\boldsymbol{R}} = \boldsymbol{R}_e \boldsymbol{R}_d^T$. The angular velocity error is then defined as $\widetilde{\boldsymbol{\omega}}_e = \boldsymbol{\omega}_e - \widetilde{\boldsymbol{R}}\boldsymbol{\omega}_d$, where $\boldsymbol{\omega}_d$ is the desired angular velocity.

Since the target admittance model (8) guarantees the RCM constraint satisfaction ensuring identically zero position and velocities in the constrained space, we can express the tip velocity with respect to the unconstrained velocities which in our case include joint velocities of the articulated tool, as follows :

$$\begin{bmatrix} \dot{\boldsymbol{p}}_e \\ \boldsymbol{\omega}_e \end{bmatrix} = \boldsymbol{J}_l \begin{bmatrix} \dot{\boldsymbol{x}}_f \\ \dot{\boldsymbol{q}}_\alpha \end{bmatrix} \tag{11}$$

where $\boldsymbol{J}_l = \boldsymbol{J}_e \begin{bmatrix} \boldsymbol{Z}^T & \boldsymbol{0}_{n\times m} \\ \boldsymbol{0}_{m\times(n-2)} & \boldsymbol{I}_{m\times m} \end{bmatrix} \in \mathbb{R}^{6\times(n+m-2)}$ is the Jacobian matrix which maps the tip's velocity to the unconstrained space velocities. The left pseudoinverse $\boldsymbol{J}_l^\dagger = \boldsymbol{J}_l^T(\boldsymbol{J}_l\boldsymbol{J}_l^T)^{-1} \in \mathbb{R}^{(n+m-2)\times 6}$ is defined away from singularities, i.e. $\boldsymbol{J}_l\boldsymbol{J}_l^\dagger = \mathbb{I}_{6\times 6}$.

Differentiating (11) yields:

$$\begin{bmatrix} \ddot{\boldsymbol{p}}_e \\ \dot{\boldsymbol{\omega}}_e \end{bmatrix} = \dot{\boldsymbol{J}}_l \begin{bmatrix} \dot{\boldsymbol{x}}_f \\ \dot{\boldsymbol{q}}_\alpha \end{bmatrix} + \boldsymbol{J}_l \begin{bmatrix} \ddot{\boldsymbol{x}}_f \\ \ddot{\boldsymbol{q}}_\alpha \end{bmatrix} \tag{12}$$

The unconstrained dynamics can then be determined by appropriately designing the term $\boldsymbol{u}_c \in \mathbb{R}^{n-2}$ in (8) and the term $\boldsymbol{u}_\alpha \in \mathbb{R}^m$ which determines the articulated tool dynamics :

$$\ddot{\boldsymbol{q}}_\alpha = \boldsymbol{u}_\alpha \tag{13}$$

The following terms are proposed to achieve the oriented path tracking objective:

$$\begin{bmatrix} \boldsymbol{u}_c \\ \boldsymbol{u}_\alpha \end{bmatrix} = \boldsymbol{J}_l^\dagger \left(\boldsymbol{F} - \dot{\boldsymbol{J}}_l \begin{bmatrix} \dot{\boldsymbol{x}}_f \\ \dot{\boldsymbol{q}}_\alpha \end{bmatrix} \right) \in \mathbb{R}^{n+m-2} \tag{14}$$

with

$$\boldsymbol{F} = \begin{bmatrix} \ddot{\boldsymbol{p}}_d \\ \frac{d(\widetilde{\boldsymbol{R}}\boldsymbol{\omega}_d)}{dt} \end{bmatrix} - \boldsymbol{D} \begin{bmatrix} \dot{\boldsymbol{p}}_e - \dot{\boldsymbol{p}}_d \\ \boldsymbol{\omega}_e - \widetilde{\boldsymbol{R}}\boldsymbol{\omega}_d \end{bmatrix} - \boldsymbol{K} \begin{bmatrix} \boldsymbol{p}_e - \boldsymbol{p}_d \\ \boldsymbol{e}_q \end{bmatrix} \tag{15}$$

where $\boldsymbol{D}$, $\boldsymbol{K}$ are diagonal matrices of damping and stiffness gains ($\boldsymbol{D} = diag([d_1\mathbf{I}_{3\times3}, d_2\mathbf{I}_{3\times3}])$, $\boldsymbol{K} = diag([k_1\mathbf{I}_{3\times3}, k_2\mathbf{I}_{3\times3}])$). Integrating (8) and (13) utilising u_c and u_a respectively from (14), generates the joint position and velocity trajectories for the whole kinematic chain.

To reveal the achievement of the oriented path tracking objective, notice that substituting (14), (15) in place of the unconstrained accelerations in (12), yields the following error dynamics in the task space:

$$\ddot{\widetilde{\boldsymbol{p}}}_e + d_1\dot{\widetilde{\boldsymbol{p}}}_e + k_1\widetilde{\boldsymbol{p}}_e = \boldsymbol{0}_{3\times3} \tag{16}$$

$$\dot{\widetilde{\boldsymbol{\omega}}}_e + d_2\widetilde{\boldsymbol{\omega}}_e + k_2\boldsymbol{e}_q = \boldsymbol{0}_{3\times3} \tag{17}$$

The linear homogeneous differential equation (16) guarantees exponential convergence of the position tracking error and the same is true for the orientation error dynamics governed by (17) as proved in [9].

V. Simulation tool and Evaluation metrics

The developed simulation tool integrates the target admittance model developed in the previous section which achieves the tracking of the planned trajectory for the instrument tip with duration t_o in N discrete steps, given a candidate incision point (RCM) $\boldsymbol{p}_c$. Surgeons can specify a region of interest in the human body, in which the incision point is opted. This surface is discretized with a step of 1cm to provide the candidate incision points for evaluation. The simulation tool iterates through the candidate incision points, evaluating the simulation results on the basis of an evaluation metric which is described below. The outcome is the best incision point that should be selected in the real operation.

We propose an evaluation function which takes into consideration parameters related to distance from sensitive areas, pressure exerted from the robotic chain at the tumor and robot's isotropy.

1) *Repulsive Forces*: In many works in the literature virtual fixtures (VF) or active constraints are associated with sensitive regions that should be protected during the operation. In our previous work for hands-on robotic surgery [3], [10], [11] we enforced such VF on the surface of a forbidden area, constructed from overlapping spheres of radius d_c centered at the cloud points $\boldsymbol{p}_{r_i}$, $i = 1, ..., M$ of the forbidden area, via barrier artificial potentials. These potentials produce repulsive forces as feedback to the surgeon during the operation when he drives the tool close to the forbidden region within a prespecified distance d_0.

In this work we propose to use these forces as an evaluation metric of the distance from sensitive areas. For each center $\boldsymbol{p}_{r_i}$, we find the closest point on each link of the articulated tool $\boldsymbol{p}_{i,k}^*$ following the algorithm introduced in [12] and calculate the repulsive force $\boldsymbol{f}_{r_{i,k}}$ from the following equation [12]:

$$\boldsymbol{f}_{r_{i,k}} = \begin{cases} \frac{k}{d_0^2(1-\psi_i)} \ln\left(\frac{1}{1-\psi_i}\right) \boldsymbol{e}_{i,k}, & ||\boldsymbol{p}_{r_i} - \boldsymbol{p}_{i,k}^*|| \le d_c + d_0 \\ \boldsymbol{0}_{3\times1}, & ||\boldsymbol{p}_{r_i} - \boldsymbol{p}_{i,k}^*|| > d_c + d_0 \end{cases} \tag{18}$$

with $\psi_i = \left(\frac{d_0 + d_c - ||\boldsymbol{p}_{i,k}^* - \boldsymbol{p}_{r_i}||}{d_0}\right)^2$ and $\boldsymbol{e}_i \in \mathbb{R}^3$ be the direction of the repulsive force:

$$\boldsymbol{e}_{i,k} = (d_0 + d_c - ||\boldsymbol{p}_{i,k}^* - \boldsymbol{p}_{r_i}||) \frac{\boldsymbol{p}_{i,k}^* - \boldsymbol{p}_{r_i}}{||\boldsymbol{p}_{i,k}^* - \boldsymbol{p}_{r_i}||} \tag{19}$$

where $k = 0, 1, ..., m$ is the articulated tool link number with $k = 0$ denoting the tool shaft. Notice that the repulsive force is non-linearly increasing as we move closer to the forbidden region surface and zero outside the activation distance d_0. Hence any solution that minimizes a metric on these forces is desirable.

At each simulation step ϕ, the total effect of all points M of the forbidden region point cloud in the unconstrained space and in the joints of the articulated instrument is expressed by the following generalized force :

$$\boldsymbol{F}_{r,\phi} = \sum_{i=1}^{M} \sum_{k=0}^{m} \boldsymbol{G}_{k,i} \boldsymbol{f}_{r_{i,k}} \in \mathbb{R}^{(4+m)} \tag{20}$$

where

$$\boldsymbol{G}_{k,i} = \begin{cases} \begin{bmatrix} \boldsymbol{x}_w^T \\ (\boldsymbol{p}_{i,k}^* - \boldsymbol{p}_c)^\wedge \\ \boldsymbol{0}_{m\times 3} \end{bmatrix}, & \text{for } k = 0 \\ \begin{bmatrix} \boldsymbol{x}_w^T \\ (\boldsymbol{p}_{i,k}^* - \boldsymbol{p}_c)^\wedge \\ \boldsymbol{J}_k^T \begin{bmatrix} \mathbf{I}_{3\times 3} \\ (\boldsymbol{p}_{i,k}^* - \boldsymbol{p}_k)^\wedge \end{bmatrix} \\ \boldsymbol{0}_{(m-k)\times 3} \end{bmatrix}, & \text{otherwise} \end{cases} \tag{21}$$

with $\boldsymbol{p}_k$ being the position of the end of the $k-th$ link w.r.t. the robot base frame and $\boldsymbol{J}_k = diag_{block}\{\boldsymbol{R}_s, \boldsymbol{R}_s\}\boldsymbol{J}_{sk} \in \mathbb{R}^{6\times k}$ be the Jacobian matrix of the articulated tool that provides the relation between the first k joint velocities $\dot{\boldsymbol{q}}_{a_{\{1:k\}}}$ and the generalized velocity of the end of the $k-th$ link w.r.t. the robot base frame.

Let us define the sets $\mathcal{K}_c, \mathcal{K}_\tau, \mathcal{K}_a$ related to repulsive force evaluation metrics in all steps of a simulation run for a candidate $\boldsymbol{p}_c$. The first contains the absolute values of the repulsive force along the shaft axis, i.e., $\mathcal{K}_c = \{|\boldsymbol{F}_{r,\phi}\{1:1\}|,\ \forall\phi = 1, ..., N\}$, the second contains the norm of the repulsive torque around the incision point, i.e., $\mathcal{K}_\tau = \{||\boldsymbol{F}_{r,\phi}\{2:4\}||,\ \forall\phi = 1, ..., N\}$ and the last set includes the norm of the repulsive torques on the articulated tool joints, i.e., $\mathcal{K}_a = \{||\boldsymbol{F}_{r,\phi}\{5:m+4\}||,\ \forall\phi = 1, ..., N\}$. The repulsive force evaluation metric is then calculated as follows:

$$F_f = \left(\frac{max\{\mathcal{K}_c\}^2 + \overline{\mathcal{K}_c}^2}{w_x}\right) + \left(\frac{max\{\mathcal{K}_\tau\}^2 + \overline{\mathcal{K}_\tau}^2}{w_\tau}\right) + \left(\frac{max\{\mathcal{K}_a\}^2 + \overline{\mathcal{K}_a}^2}{w_a}\right) \tag{22}$$

where the operator $\overline{(...)}$ denotes the mean value and max is the max member of the set and w_x, w_τ and w_a are weights to account for the different units of the elements of the above summation.

2) *Pressure Distance*: In some surgical cases, inadvertent contact with a tumor creates accidental cuts in its surface. Hence, we introduce an evaluation metric which we call pressure distance, which should be minimized to avoid such incidences. In particular, pressure distance is defined as the maximum deformation caused by any link of the articulated tool during the simulation run which would exert pressure to the tumor and may injure it during the operation. Let the pressure distance be denoted $\delta_{k,\phi} \in \mathbb{R}_{\geq} 0,\ k = 0, 1, ..., m$. To calculate these values from a given point cloud of a tumor we can either utilize tumor enclosure geometrical shapes like spheres or find the maximum distance between the points of the deformed by the link tumor point cloud from the non-deformed one. The total pressure from all links is: $f_{\delta,\phi} = \sum_{k=0}^{m} \delta_{k,\phi}$.

Let us define the set $\mathcal{K}_\delta$, that includes the sum of the pressure from all links in all steps of a simulation run, i.e., $\mathcal{K}_\delta = \{f_{\delta,\phi},\ \forall\phi = 1, ..., N\}$. We then define the pressure distance evaluation metric as follows:

$$F_\delta = \left(\frac{max\{\mathcal{K}_\delta\}}{w_\delta}\right)^2 + \left(\frac{\overline{\mathcal{K}_\delta}}{w_\delta}\right)^2 \tag{23}$$

The weight w_δ denotes the tumor deformation from inadvertent contact that is considered critical for injury and accidental cuts on its surface.

3) *System's Isotropy*: The isotropy of the Jacobian matrix $\boldsymbol{J}_e$ provides a measure for the robotic's chain kinematic accuracy. A redundant manipulator is isotropic if all of the singular values of the Jacobian $\boldsymbol{J}_e$ are identical and non-zero at a specific configuration [13]. One measure of the isotropy is the ratio below:

$$\kappa_\phi(\boldsymbol{J}_e) = \frac{\sigma_M(\boldsymbol{J}_e)}{\sigma_m(\boldsymbol{J}_e)} \tag{24}$$

where σ_M and σ_m are the maximum and the minimum singular value of the $\boldsymbol{J}_e$. Let us define the set $\mathcal{K}_\kappa$, that includes the isotropy measure in all steps of a simulation run, i.e., $\mathcal{K}_\kappa = \{\kappa_\phi,\ \forall\phi = 1, ..., N\}$. Note that the greater this ratio is, the robotic chain is closer to singularity, and the closer this ration is to one, the further the robotic chain is away from singularity. Hence, we define the term F_κ, as follows:

$$F_\kappa = \big(max\{\mathcal{K}_\kappa\}\big)^2 + \big(\overline{\mathcal{K}_\kappa}\big)^2 \tag{25}$$

Finally, the optimization function F for evaluating the candidate incision points is described below:

$$F = F_f + F_\delta + F_\kappa \tag{26}$$

VI. RESULTS

In this paper, we consider the kinematic model of $n = 7$-dof KUKA LWR4+ robotic manipulator holding a surgical tool. The surgical tool consists of a shaft of length $L = 25\ cm$ and an articulated instrument with $m = 2$ rotational dof with 2 links of length $1\ cm$ see Fig. 2. We consider the emulation of a tumor resection in partial nephrectomy. The patient in this type of operation is placed in a modified flank position of 45^o as proposed in [14]. The simulated intraoperative environment consists of the right kidney with a tumor (green area in Fig. 3) and the lower layers of the liver that are characterized as forbidden area, (red area in

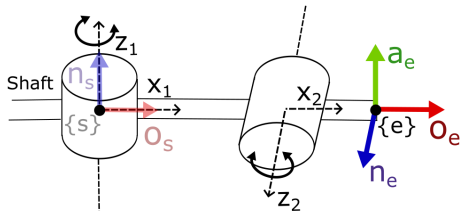

Fig. 2. The articulated tool with two rotational joints with perpendicular axes shown at zero joint angles

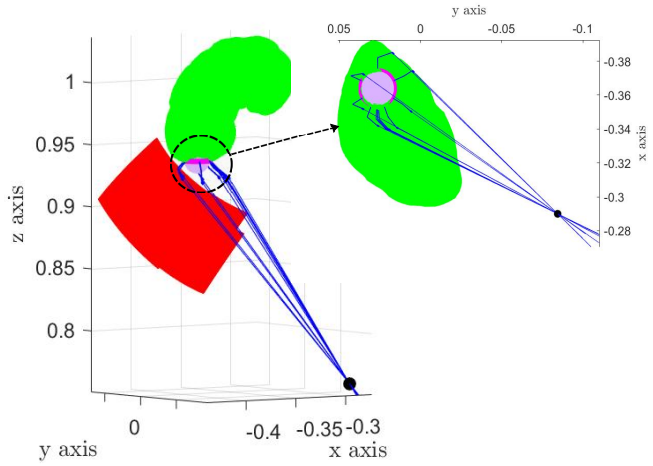

Fig. 3. Trace of the tool for the optimal incision point. The kidney is represented with green, the sensitive areas with red, the tumor with pink, and the desired path with magenta.

Fig. 3). The tumor is enclosed in a sphere with radius $\rho = 1\ cm$ indicated with magenta color at Fig. 3. The planned oriented path is circular with the same center as the tumor and tangential to the local geometry of the kidney with radius $1.1\ cm$ and the planned orientation requires the final tool link axis to remain in an angle of 45^o with the circular trajectory's plane. The pressure distance $\delta_{k,\phi}$ for each link is given by:

$$\delta_{k,\phi} = \begin{cases} \rho - \alpha_t & \text{if } \rho \geq \alpha_t \\ 0 & \text{else} \end{cases} \in \mathbb{R} \qquad (27)$$

where α_t is the minimum distance between the link surface and the center of the sphere. The algorithm used to find the closest point is provided in [12]. The candidate incision points $\boldsymbol{p}_{c_m}$ is a 60-point rectangular grid determined by the surgeon, close to the umbilical cord, as proposed in [15] and seen in Fig. 4. Grid candidate incision points are given by:

$$\boldsymbol{p}_{c_m} = \boldsymbol{p}_u + [0;\ 0.01y_r;\ 0.01z_r]^T\ m$$
$$1 \leq y_r \leq 10,\ 1 \leq z_r \leq 6,\ \ y_r, z_r \in \mathbb{N} \qquad (28)$$

where $\boldsymbol{p}_u = [-0.29;\ -0.0944;\ 0.75]^T\ m$ is the center of the umbilical cord.

The selected parameter values are $d_c = 2\ mm$ for the point cloud spheres to cover the empty space, $d_0 = 4.25\ mm, k = 1$, for the repulsive force activation distance and gain, $a = 50$, $k_1 = 1000$, $k_2 = 500$, $d_1 = 63.2$, $d_2 = 44.7$, for a fast and critically damped dynamics in the constraint and free

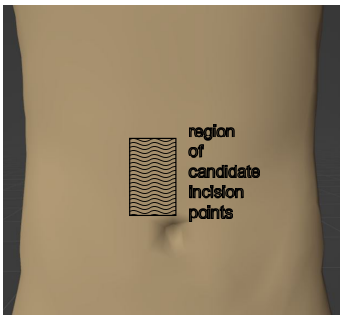

Fig. 4. The region of the candidate incision points selected by surgeon.

space and $w_x = 10$, $w_\tau = 2$, $w_\alpha = 0.15$ and $w_\delta = 0.001$ for weighting evaluation metric components.

We run the simulation tool for all candidate incision points and calculated the evaluation metric. Alternative an optimization method e.g. genetic algorithms could be used but as the set of candidate points is not excessive and the process is offline an exhaustive search is satisfactory. Fig. 3 shows the trace of the tool during the task, given a specific incision point. As expected, the oriented path is tracked by the instrument tip and the RCM constraint with the RCM denoted by a black dot is full-filled. Fig. 5a-d show the evaluation metric F and its components, F_f, F_δ, F_κ respectively. For better scaling, the logarithmic function is utilized. From Fig. 5 is clear that the optimal point is in the corner of the search area with coordinates $(y_r, z_r) = (1, 1)$ and with value $F = 806.43$. This point is also the optimal for each evaluation metric F_f, F_δ, F_κ; see Fig. 5b-d. The simulation model detects incision points at which the sensitive area is violated, which are excluded from evaluation. In Fig 5a-d, they are marked by red and lie near the two sides of the grid area. Fig. 5b shows that the evaluation metric F_f for the rest of the candidate incision points which decreases when approaching the optimal point at which the value is zero. This indicates that at the optimal point the whole tool stays away from the forbidden region at a distance greater than d_0. Any suboptimal point with non-zero value of F_f means that the surgeon would feel repulsive forces at segments of the operation path obstructing his work. The evaluation metric F_δ for the pressure distance is decreasing near the same corner, as shown in Fig. 5c. This happens because in this region the motion of the articulated tool tracking the oriented path, is more blunt w.r.t trajectory's plane. As a result, the tumor is not pressed in the optimal incision point and the surgical task can be achieved without inadvertent contact that may cause cancer metastasis. The same reduction in the evaluation metric F_k is observed, as seen in Fig. 5d, with the most beneficial isotropy of max value 25.4 and mean value of 12.7 achieved at the optimal.

VII. CONCLUSIONS

In this work, we propose a preoperative simulation tool for finding the optimal incision point in robot assisted minimally invasive surgery which guarantees minimal intraoperative

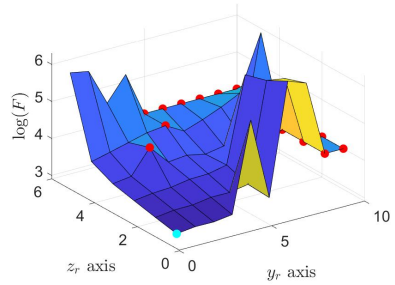

(a) Optimization function F.

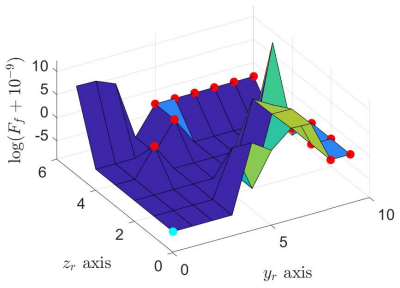

(b) Evaluation metric F_f.

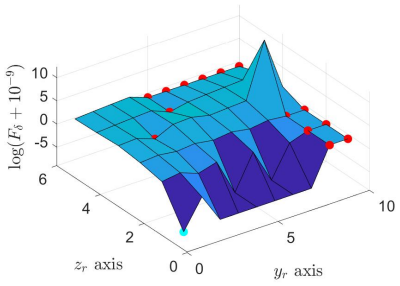

(c) Evaluation metric F_δ.

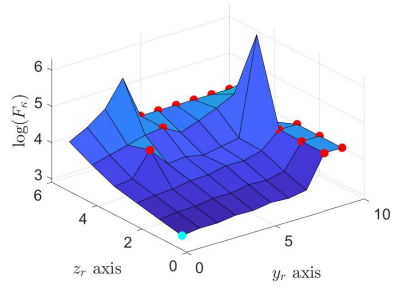

(d) Evaluation metric F_κ.

Fig. 5. Evaluation metrics F, F_f, F_δ, F_κ. The optimal incision point is shown with cyan color. The incision points in which sensitive area is violated are shown in red. Constant 10^{-9} is used for points with zero metric value.

risks and safe task execution. The tool simulates the tracking of a preplanned oriented path from the proposed target admittance model which respects RCM constraints. For each run it calculates the cost value according to the proposed evaluation metrics. Results demonstrate the utilization of such a tool in the preoperative stage by indicating candidate incisions that cause violation of the sensitive area when the path is faithfully tracked and the optimal location that would facilitate the work of the surgeon during the operation. The simulation tool can be tailored to the kinematics of different general purpose manipulators and articulated tools. It also provides the possibility to prioritize the calculated metrics by changing the weights of the cost function. Future work will improve the simulation model by including more metrics that may be of interest to a surgeon and extensive use in various surgical cases.

REFERENCES

[1] C.-H. Kuo, J. S. Dai, and P. Dasgupta, "Kinematic design considerations for minimally invasive surgical robots: an overview," *The International Journal of Medical Robotics and Computer Assisted Surgery*, vol. 8, no. 2, pp. 127–145, 2012.

[2] T. Kastritsi and Z. Doulgeri, "A controller to impose a rcm for hands-on robotic-assisted minimally invasive surgery," *IEEE Transactions on Medical Robotics and Bionics*, vol. 3, no. 2, pp. 392–401, 2021.

[3] ——, "A passive admittance controller to enforce remote center of motion and tool spatial constraints with application in hands-on surgical procedures," *Robotics and Autonomous Systems*, vol. 152, p. 104073, 2022.

[4] R. C. Locke and R. V. Patel, "Optimal remote center-of-motion location for robotics-assisted minimally-invasive surgery," in *Proceedings 2007 IEEE International Conference on Robotics and Automation*. IEEE, 2007, pp. 1900–1905.

[5] F. Cursi and P. Kormushev, "Pre-operative offline optimization of insertion point location for safe and accurate surgical task execution," in *2021 IEEE/RSJ International Conference on Intelligent Robots and Systems (IROS)*. IEEE, 2021, pp. 4040–4047.

[6] G. Li, C. Zhi, D. Zhu, Z. Liu, and Y. Niu, "Efficacy of povidone-iodine against accidental tumor incision during nephron-sparing surgery: experimental study in patients with renal cell carcinoma," *Journal of International Medical Research*, vol. 47, no. 10, pp. 4993–5002, 2019.

[7] P. L. Anderson, R. A. Lathrop, and R. J. Webster III, "Robot-like dexterity without computers and motors: a review of hand-held laparoscopic instruments with wrist-like tip articulation," *Expert review of medical devices*, vol. 13, no. 7, pp. 661–672, 2016.

[8] T. Kastritsi and Z. Doulgeri, "A passive control framework for a bilateral leader-follower robotic surgical setup imposing rcm and active constraints," in *2022 IEEE/RSJ International Conference on Intelligent Robots and Systems (IROS)*, 2022, pp. 1175–1181.

[9] L. Koutras and Z. Doulgeri, "Exponential stability of trajectory tracking control in the orientation space utilizing unit quaternions," in *2021 IEEE/RSJ International Conference on Intelligent Robots and Systems (IROS)*. IEEE, 2021, pp. 8151–8158.

[10] T. Kastritsi, D. Papageorgiou, I. Sarantopoulos, Z. Doulgeri, and G. A. Rovithakis, "Stability of active constraints enforcement in sensitive regions defined by point-clouds for robotic surgical procedures," in *2019 18th European Control Conference (ECC)*. IEEE, 2019, pp. 1604–1609.

[11] T. Kastritsi, D. Papageorgiou, I. Sarantopoulos, S. Stavridis, Z. Doulgeri, and G. A. Rovithakis, "Guaranteed active constraints enforcement on point cloud-approximated regions for surgical applications," in *2019 International Conference on Robotics and Automation (ICRA)*. IEEE, 2019, pp. 8346–8352.

[12] T. Kastritsi, I. Sarantopoulos, S. Stavridis, D. Papageorgiou, and Z. Doulgeri, "Manipulation of a whole surgical tool within safe regions utilizing barrier artificial potentials," in *Mediterranean Conference on Medical and Biological Engineering and Computing*. Springer, 2019, pp. 1559–1570.

[13] A. Trejos, R. Patel, I. Ross, and B. Kiaii, "Optimizing port placement for robot-assisted minimally invasive cardiac surgery," *The International Journal of Medical Robotics and Computer Assisted Surgery*, vol. 3, no. 4, pp. 355–364, 2007.

[14] J. H. Kaouk and R. K. Goel, "Single-port laparoscopic and robotic partial nephrectomy," *European urology*, vol. 55, no. 5, pp. 1163–1170, 2009.

[15] J. D. Raman, A. Bagrodia, and J. A. Cadeddu, "Single-incision, umbilical laparoscopic versus conventional laparoscopic nephrectomy: a comparison of perioperative outcomes and short-term measures of convalescence," *European urology*, vol. 55, no. 5, pp. 1198–1206, 2009.